A Synthetic Model of the Mn_3Ca Subsite of the Oxygen-Evolving Complex in Photosystem II

Jacob S. Kanady *et al.*

Science **333**, 733 (2011);
DOI: 10.1126/science.1206036

17. K. G. Makris, R. El-Ganainy, D. N. Christodoulides, Z. H. Musslimani, *Phys. Rev. Lett.* **100**, 103904 (2008).
18. R. El-Ganainy, K. G. Makris, D. N. Christodoulides, Z. H. Musslimani, *Opt. Lett.* **32**, 2632 (2007).
19. Z. H. Musslimani, K. G. Makris, R. El-Ganainy, D. N. Christodoulides, *Phys. Rev. Lett.* **100**, 030402 (2008).
20. A. Guo *et al.*, *Phys. Rev. Lett.* **103**, 093902 (2009).
21. C. E. Rüter *et al.*, *Nat. Phys.* **6**, 192 (2010).
22. Materials and methods are available as supporting material on *Science* Online.
23. M. Abashin *et al.*, *Opt. Express* **14**, 1643 (2006).
24. B. Liang, X. S. Guo, J. Tu, D. Zhang, J. C. Cheng, *Nat. Mater.* **9**, 989 (2010).

Acknowledgments: Support by NSF and NSF ERC Center for Integrated Access Networks grant EEC-0812072, Defense Advanced Research Projects Agency under the Nanoscale Architecture for Coherent Hyperoptical Sources program grant W911NF-07-1-0277, National Basic Research Program of China grant 2007CB613202, National Nature Science Foundation of China grants 50632030 and 10874080, and Nature Science Foundation of Jiangsu Province grant BK2007712. We thank Nanonics, Ltd., for extensive training and support in near-field scanning optical microscopy. M.A. acknowledges support of a Cymer Corp. graduate fellowship.

Supporting Online Material
www.sciencemag.org/cgi/content/full/333/6043/729/DC1
Materials and Methods
Figs. S1 to S3
References

24 March 2011; accepted 27 June 2011
10.1126/science.1206038

A Synthetic Model of the Mn_3Ca Subsite of the Oxygen-Evolving Complex in Photosystem II

Jacob S. Kanady, Emily Y. Tsui, Michael W. Day, Theodor Agapie*

Within photosynthetic organisms, the oxygen-evolving complex (OEC) of photosystem II generates dioxygen from water using a catalytic Mn_4CaO_n cluster (*n* varies with the mechanism and nature of the intermediate). We report here the rational synthesis of a $[Mn_3CaO_4]^{6+}$ cubane that structurally models the trimanganese-calcium–cubane subsite of the OEC. Structural and electrochemical comparison between Mn_3CaO_4 and a related Mn_4O_4 cubane alongside characterization of an intermediate calcium-manganese multinuclear complex reveals potential roles of calcium in facilitating high oxidation states at manganese and in the assembly of the biological cluster.

Biological dioxygen generation occurs at the oxygen-evolving complex (OEC) of photosystem II (PSII) in cyanobacteria and plants (*1*). The active site responsible for this transformation consists of a Mn_4CaO_n cluster (*n* varies with the mechanism and nature of the intermediate) embedded in a large protein complex (*2*–*8*). One commonly proposed arrangement of metals in the active site is three closely spaced manganese centers, part of a heteronuclear Mn_3CaO_4 cubane, bridging via oxide or hydroxide ligands to a dangling fourth manganese (*2*–*9*). Given broad fundamental interest and potential applications in artificial photosynthesis, the structure of this cluster and the mechanism of water splitting to make dioxygen have been the subject of many spectroscopic, computational, synthetic, crystallographic, and biochemical studies (*1*, *10*–*12*). Despite major advances, the mechanism of oxygen production is not well understood. During one turnover, four oxidizing equivalents generated by light are delivered to the active-site cluster, leading to the stepwise formation of intermediates commonly referred to as the S states. The sequential transitions from S_0 (the most reduced state) to S_4 (the most oxidized state) involve electron- and proton-transfer events. The highly oxidized S_4 state is unstable and evolves dioxygen to return to the S_0 state. The exact Mn oxidation states and the site of O-O bond formation in S_4 are debated; nevertheless, high–oxidation state Mn centers are required to activate a terminal or bridging oxo ligand for O_2 production. The large protein matrix has complicated direct studies of the OEC active site, and the synthesis of small-molecule models has been impeded by the complexity of the cluster.

The synthesis of potentially biomimetic manganese oxide clusters has relied heavily on self-assembly because of the propensity of oxide and hydroxide ligands to bridge two or more metal centers (*13*). Judicious choice of ancillary ligands has enabled synthesis of a large variety of manganese clusters (*13*–*16*). Some of these complexes have provided valuable spectroscopic models for the OEC as well as insight into the reactivity of high–oxidation state manganese species, including water oxidation (*17*, *18*). The synthesis of an accurate model of the full active-site cluster has been elusive, however. Many di-, tri-, and tetranuclear clusters of manganese with bridging oxides have been reported (*16*), but incorporation of a calcium center is much less common (*19*–*24*). Although they incorporate a cuboidal arrangement, the reported Ca-Mn clusters are of much higher nuclearity than the OEC (*19*, *21*). Thus, fundamental studies on the role of calcium have been hindered by a lack of well-defined, small-molecule models.

To access heteronuclear clusters of predictable structure, we employed a recently developed trinucleating ligand framework. This architecture consists of a rigid 1,3,5-triarylbenzene spacer incorporating six pyridine and three alcohol groups (**1-H$_3$**, Fig. 1) (*25*, *26*). Reaction with three equivalents of manganese (II) acetate in the presence of base leads to the formation of a yellow trinuclear manganese complex, **2**, supported by pyridine donors and bridging alkoxides. Three capping acetates complete the coordination sphere of the metals. This trimetallic platform was envisioned as a precursor for the synthesis of more complex clusters.

Targeting a heterotetranuclear complex containing calcium and manganese, we treated **2** with two equivalents of potassium superoxide as a source of both oxygen atoms and oxidizing equivalents in the presence of $Ca(OTf)_2$ (OTf, trifluoromethanesulfonate) (Fig. 1). Although **2** is insoluble in tetrahydrofuran (THF), addition of $Ca(OTf)_2$ leads to partial dissolution of the suspended material, suggesting the formation of a more soluble Ca-Mn intermediate. Reaction with superoxide over 24 to 48 hours leads to the formation of a brown, heterogeneous mixture with a purple precipitate. Filtration affords a purple solid (**5**)—characterized by single-crystal x-ray diffraction (XRD) as a calcium-hexamanganese cluster in which two monooxygenated Mn_3 cores are linked to Ca^{2+} via acetate bridges (fig. S7)—and a brown supernatant. Vapor diffusion of hexane into the THF supernatant afforded red-brown crystals of compound **4**, which was also characterized by XRD. Compound **4** displays the desired $[Mn_3CaO_4]^{6+}$ core (Fig. 2, A and B). The three manganese centers are supported by framework **1**, with each manganese binding to one alkoxide and one pyridyl group; three pyridyl groups from **1** remain unbound. The manganese centers are pseudo-octahedral, and the calcium center is supported by three oxide ligands and three acetates that bridge across different faces of the cube. The calcium coordination sphere is completed by a THF molecule, consistent with a large heptacoordinate calcium center. Modeling all four metal sites as manganese centers does not fit the XRD data, and the Ca–O distances are all considerably longer than would be expected for Mn–O bonds (table S2). Analysis of the Mn-oxo distances in **4** reveals short average bond lengths of 1.87 Å, consistent with three Mn^{IV} centers. In agreement with this oxidation-state assignment, the standard deviation of the Mn-oxo bond lengths is small, as expected for a d^3 electronic configuration.

Department of Chemistry and Chemical Engineering, California Institute of Technology, 1200 East California Boulevard MC 127-72, Pasadena, CA 91125, USA.

*To whom correspondence should be addressed. E-mail: agapie@caltech.edu

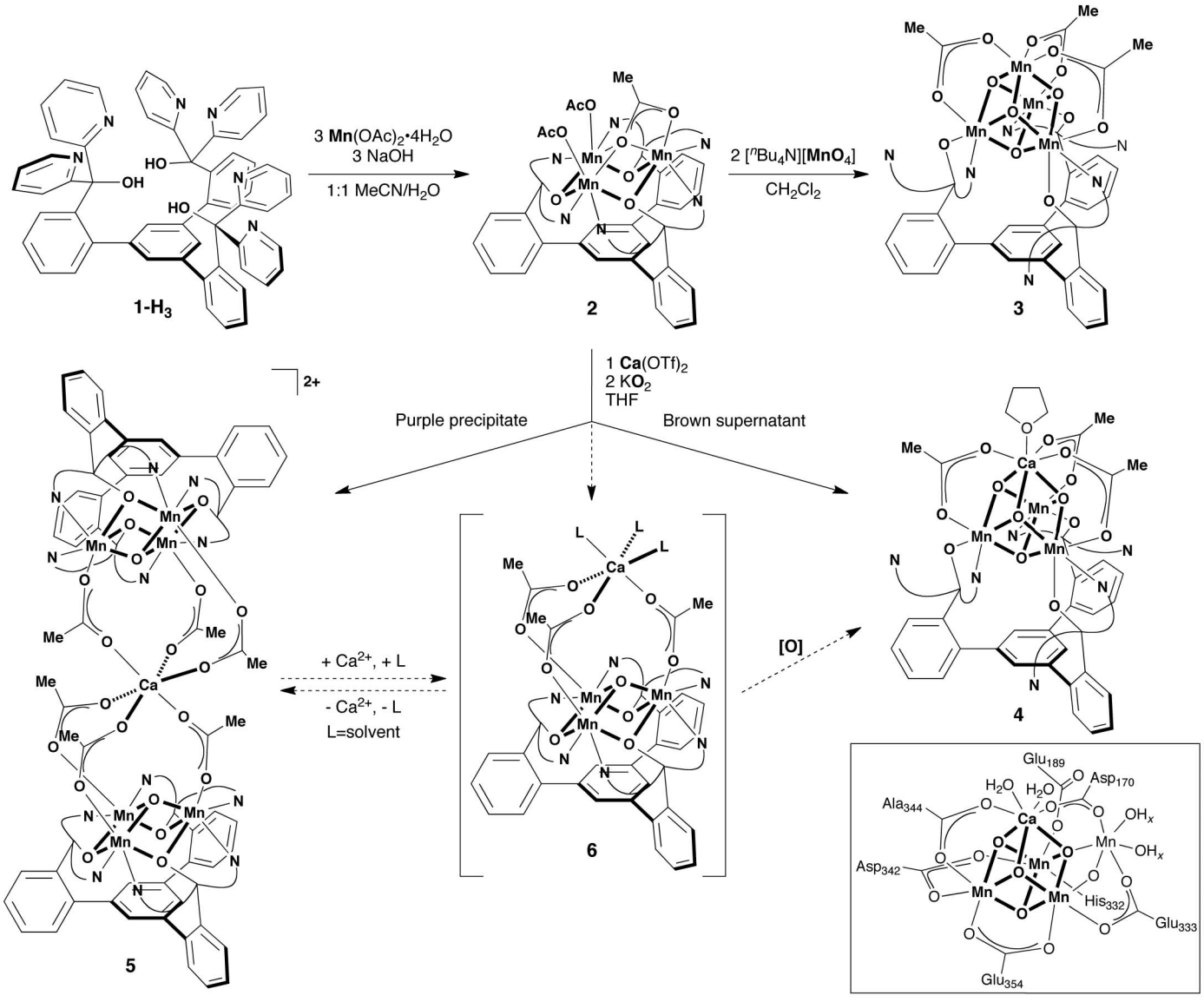

Fig. 1. Synthesis of **2**, **3**, **4**, and **5** from **1-H$_3$** and proposed formation of an intermediate (**6**). Curved lines in structures schematically represent 2-pyridyl groups. (**Inset**) A recent structure of the OEC from crystallographic studies is shown (*8*). OAc/AcO, acetoxy group; Me, methyl; Bu, butyl.

The discrete [Mn_3CaO_4] core matches the proposed structure of PSII without the dangler manganese. The Mn–Mn distances and Mn–Ca distances of **4** parallel those found in extended x-ray absorption fine structure (EXAFS) and crystallographic studies of PSII (*7*, *8*, *11*, *27*). The average Mn–Mn distance in **4** is 2.834 Å, and the average Mn–Ca distance is 3.231 Å. A recent crystallographic study gave Mn–Mn distances of 2.8, 2.9, and 3.3 Å and Mn–Ca distances of 3.3, 3.4, and 3.5 Å within the cubane subsite. (*8*) The corresponding EXAFS-derived distances in PSII are 2.7 to 3.2 Å and 3.3 to 3.4 Å in the S_1 state (*7*, *11*, *27*). The shorter Mn–Ca distance observed in **4** may be a consequence of bridging constraints caused by three acetate bridges, whereas in proposed structures of the OEC, the Ca^{2+} has more open coordination (*8*). There has been debate over the oxidation states of the manganese centers in the OEC (*1*, *28*, *29*). The three Mn centers of the cubane subsite have been proposed to be in the +IV oxidation state in the S_2, S_3, and S_4-states (*28*, *29*). The three manganese centers in **4** are all in the oxidation state +IV (vide supra), supporting [$Mn^{IV}{}_3CaO_4$] as a feasible structure in the latter stages of the S-state cycle. The isolation of **4** in the solid state at room temperature suggests that the heteronuclear cubane motif is stable and does not require a fully encapsulating ligand like that provided by the protein environment.

A related Mn_4O_4 cubane could give insight into the distinct properties calcium elicits from a multinuclear manganese cluster. When **2** was treated with two equivalents of $^nBu_4NMnO_4$, we observed a brown tetranuclear manganese complex (**3**) (Fig. 1) (*30*). Compound **3** was characterized by XRD and contains a Mn_4O_4 cubane core analogous to **4** (Fig. 2C). The structural parameters are consistent with the presence of two d^3 Mn^{IV} centers, displaying short, similar Mn–O bonds and two d^4 Mn^{III} centers with longer, distorted Mn–O coordination (table S2). Complexes **3** and **4** were investigated by cyclic voltammetry in dimethylacetamide (DMA) and dimethylformamide (DMF) with 0.1 M $^nBu_4NPF_6$ electrolyte. Complex **4** displays a quasireversible reduction at –940 mV versus ferrocene/ferrocenium (Fc/Fc^+) in DMA (–890 mV versus Fc/Fc^+ in DMF) assigned to the [$Mn^{IV}{}_2Mn^{III}CaO_4$]/[$Mn^{IV}{}_3CaO_4$] couple (Fig. 3). Complex **3** shows a quasireversible oxidation at +290 mV versus Fc/Fc^+ assigned to the [$Mn^{IV}{}_2Mn^{III}{}_2O_4$]/[$Mn^{IV}{}_3Mn^{III}O_4$] couple and a quasireversible reduction at –700 mV in DMA assigned to the [$Mn^{IV}Mn^{III}{}_3O_4$]/[$Mn^{IV}{}_2Mn^{III}{}_2O_4$] couple (Fig. 3). The calcium-containing $Mn^{IV}{}_3CaO_4$ cubane reduces

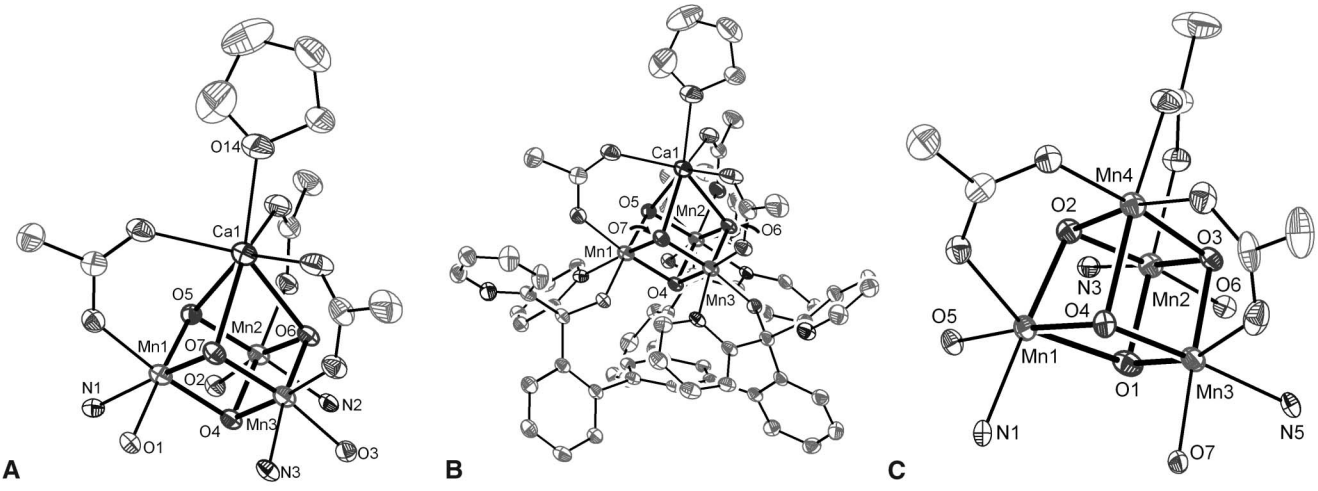

Fig. 2. Solid-state structures: (**A**) truncated Mn_3CaO_4 cubane in **4**, (**B**) full structure of **4**, and (**C**) truncated Mn_4O_4 cubane in **3**. Thermal ellipsoids are drawn at 50% probability. Hydrogen atoms and solvent molecules are not shown for clarity. Metal-oxo average distance (angstroms) and the corresponding standard deviation (in parenthesis) for each specific metal center in **3** and **4** are as follows: **3**: Mn1 2.036 (0.187), Mn2 1.864 (0.016), Mn3 1.926 (0.074), Mn4 2.012 (0.165); **4**: Mn1 1.873 (0.038), Mn2 1.872 (0.048), Mn3 1.869 (0.043), Ca1 2.417 (0.023). See table S2 for a complete list of metal-oxo and metal-metal distances.

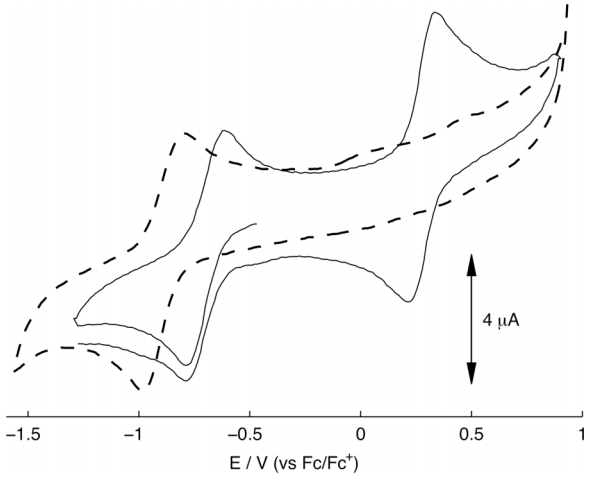

Fig. 3. Cyclic voltammograms of **3** (solid trace, DMA solution) and **4** (dashed trace, DMF solution) with 0.1 M $^{n}Bu_4NPF_6$. Scan rates: 50 mV/s (**3**) and 100 mV/s (**4**). E/V, potential.

at potentials >1 V more negative compared with the all-manganese $Mn^{IV}{}_3Mn^{III}O_4$ cluster. These data suggest that the presence of a nonredox-active calcium center, instead of manganese, facilitates the formation of a species containing more highly oxidized manganese centers at lower potentials.

Recent studies of iron-oxo species interacting with Ca^{2+} and Sc^{3+} have suggested that the redox inactive metal plays a role in facilitating reduction chemistry involving iron (*31*). The present study suggests a complementary role of Ca^{2+}. The overall charges of the cubanes in **3** and **4** are the same: $[Mn_4O_4]^{6+}$ versus $[Mn_3CaO_4]^{6+}$. The redox-inactive Ca^{2+} allows the buildup of localized positive charge, resulting in the higher oxidation state (+IV) at the three manganese centers in cluster **4**. When four redox-active metal centers are present in the same unit in **3**, the higher oxidation state is partially quenched by the formation of two Mn^{III} centers by the formal comproportionation of one Mn^{II} and one Mn^{IV}. This intriguing difference suggests that calcium may be involved in the modulation of the reduction potentials of the manganese centers in the OEC, localizing the charge and thus facilitating access to the higher oxidation states necessary for efficient O_2 production. This notion is supported by our electrochemical data showing that the calcium-containing cluster accesses the state with three Mn^{IV} centers at a substantially more negative potential compared with the all-manganese cubane. The charge-localization effect described above has been observed in high–oxidation state nickel oxides: Ternary $BaNi^{IV}O_3$ is stable, whereas simple binary Ni^{IV} oxides are unstable and generally contain Ni^{III} (*32*, *33*). More recently, a heterogeneous cobalt-oxide catalyst for water oxidation has been proposed to contain alkaline metals (albeit not detected by x-ray absorption spectroscopy) (*34*) as part of Co_3O_4 cubane moieties (*35*, *36*). The alkaline metal in this species could facilitate access to high–oxidation state cobalt species as described above. Furthermore, studies of manganese-oxide versus manganese-calcium-oxide electrocatalysts for O_2 generation from water revealed that the mixed oxide is a faster catalyst, although the exact role of calcium remained unclear (*37*).

Isolation of compound **5** in the transformation of **2** to **4** offers insight into a potential mechanism of heterometallic cubane formation. Calcium could associate to the trimanganese core via acetate bridges, explaining the mutual dissolution upon mixing in THF and opening coordination sites on the manganese centers for reaction with the oxygenation agent. Transfer of the first oxygen atom equivalent could afford proposed species **6**, which in turn could disproportionate to generate **5** and free Ca^{2+} (Fig. 1). Complexes **5** and **6** contain mixed-valence Mn^{II}-Mn^{III} sites that are located an appropriate distance from calcium for the formation of a cubane upon further reaction with oxygen-atom equivalents. This mechanism is similar to proposals based on biochemical studies for the assembly of the OEC (*38*). Mn^{2+} and Ca^{2+} are required for the biosynthesis of a functional cluster in PSII. These labile precursors are proposed to assemble in a geometry that allows for gradual hydration and photooxidation to the final cluster. In the absence of Ca^{2+}, excessive incorporation of manganese was reported, presumably due to uncontrolled oligomerization of manganese oxide species (*38*–*40*); however, recovery of activity can be achieved by subsequent addition of Ca^{2+} (*41*). Without Ca^{2+}, the assembled manganese-oxide cluster is less prone to oxidation beyond the S_2 state, further supporting a role for the redox inactive metal in facilitating access to the higher–oxidation state cluster (*41*).

Our work establishes that the discrete $[Mn_3CaO_4]$ core is synthetically accessible with the use of a trinucleating ligand architecture and a bioinspired protocol. We expect our studies to provide a better understanding of the PSII mechanism and complex cluster assembly, as well as to aid in the design of better catalysts for water splitting.

References and Notes

1. J. P. McEvoy, G. W. Brudvig, *Chem. Rev.* **106**, 4455 (2006).
2. K. N. Ferreira, T. M. Iverson, K. Maghlaoui, J. Barber, S. Iwata, *Science* **303**, 1831 (2004); 10.1126/science.1093087.
3. A. Guskov *et al.*, *Nat. Struct. Mol. Biol.* **16**, 334 (2009).
4. B. Loll, J. Kern, W. Saenger, A. Zouni, J. Biesiadka, *Nature* **438**, 1040 (2005).
5. A. Zouni *et al.*, *Nature* **409**, 739 (2001).
6. H. Dau, M. Haumann, *Coord. Chem. Rev.* **252**, 273 (2008).
7. J. Yano *et al.*, *Science* **314**, 821 (2006).
8. Y. Umena, K. Kawakami, J. R. Shen, N. Kamiya, *Nature* **473**, 55 (2011).
9. J. M. Peloquin *et al.*, *J. Am. Chem. Soc.* **122**, 10926 (2000).
10. C. W. Cady, R. H. Crabtree, G. W. Brudvig, *Coord. Chem. Rev.* **252**, 444 (2008).
11. H. Dau, A. Grundmeier, P. Loja, M. Haumann, *Philos. Trans. R. Soc. London Ser. B Biol. Sci.* **363**, 1237 (2008).
12. J. Barber, J. W. Murray, *Philos. Trans. R. Soc. London Ser. B Biol. Sci.* **363**, 1129 (2008).
13. F. A. Armstrong, *Philos. Trans. R. Soc. London Ser. B Biol. Sci.* **363**, 1263 (2008).
14. C. S. Mullins, V. L. Pecoraro, *Coord. Chem. Rev.* **252**, 416 (2008).
15. G. C. Dismukes *et al.*, *Acc. Chem. Res.* **42**, 1935 (2009).
16. G. Christou, *Acc. Chem. Res.* **22**, 328 (1989).
17. M. Yagi, M. Kaneko, *Chem. Rev.* **101**, 21 (2001).
18. S. Mukhopadhyay, S. K. Mandal, S. Bhaduri, W. H. Armstrong, *Chem. Rev.* **104**, 3981 (2004).
19. A. Mishra, W. Wernsdorfer, K. A. Abboud, G. Christou, *Chem. Commun.* **2005**, 54 (2005).
20. V. Kotzabasaki, M. Siczek, T. Lis, C. J. Milios, *Inorg. Chem. Commun.* **14**, 213 (2011).
21. A. Mishra *et al.*, *Chem. Commun.* **2007**, 1538 (2007).
22. I. J. Hewitt *et al.*, *Chem. Commun.* **2006**, 2650 (2006).
23. S. Nayak, H. P. Nayek, S. Dehnen, A. K. Powell, J. Reedijk, *Dalton Trans.* **40**, 2699 (2011).
24. Y. J. Park, J. W. Ziller, A. S. Borovik, *J. Am. Chem. Soc.* **133**, 9258 (2011).
25. E. Y. Tsui, M. W. Day, T. Agapie, *Angew. Chem. Int. Ed.* **50**, 1668 (2011).
26. E. Y. Tsui, J. S. Kanady, M. W. Day, T. Agapie, *Chem. Commun.* **47**, 4189 (2011).
27. J. Yano, V. K. Yachandra, *Inorg. Chem.* **47**, 1711 (2008).
28. J. P. McEvoy, J. A. Gascon, V. S. Batista, G. W. Brudvig, *Photochem. Photobiol. Sci.* **4**, 940 (2005).
29. J. Messinger, *Phys. Chem. Chem. Phys.* **6**, 4764 (2004).
30. Caution! Permanganate salts are potentially explosive and should be synthesized and used in small quantities.
31. S. Fukuzumi *et al.*, *Nat. Chem.* **2**, 756 (2010).
32. M. Arjomand, D. J. Machin, *J. Chem. Soc. Dalton Trans.* **1975**, 1055 (1975).
33. W. Levason, C. A. McAuliffe, *Coord. Chem. Rev.* **12**, 151 (1974).
34. M. W. Kanan *et al.*, *J. Am. Chem. Soc.* **132**, 13692 (2010).
35. M. D. Symes, Y. Surendranath, D. A. Lutterman, D. G. Nocera, *J. Am. Chem. Soc.* **133**, 5174 (2011).
36. M. W. Kanan, D. G. Nocera, *Science* **321**, 1072 (2008); 10.1126/science.1162018.
37. M. M. Najafpour, T. Ehrenberg, M. Wiechen, P. Kurz, *Angew. Chem. Int. Ed.* **49**, 2233 (2010).
38. J. E. Bartlett, S. V. Baranov, G. M. Ananyev, G. C. Dismukes, *Philos. Trans. R. Soc. London Ser. B Biol. Sci.* **363**, 1253 (2008).
39. C. G. Chen, J. Kazimir, G. M. Cheniae, *Biochemistry* **34**, 13511 (1995).
40. A. M. Tyryshkin *et al.*, *Biochemistry* **45**, 12876 (2006).
41. N. Tamura, Y. Inoue, G. M. Cheniae, *Biochim. Biophys. Acta* **976**, 173 (1989).

Acknowledgments: We thank California Institute of Technology, the Searle Scholars Program (T.A.), the Rose Hill Foundation (J.S.K.), and the NSF Graduate Research Fellowship Program (E.Y.T.) for funding. We also thank L. M. Henling for assistance with crystallography. The Bruker KAPPA APEXII x-ray diffractometer was purchased via an NSF Chemistry Research Instrumentation and Facilities: Departmental Multi-User Instrumentation award to Caltech (CHE-0639094). Crystallographic data have been deposited at the Cambridge Crystallographic Database Centre, and copies can be obtained on request, free of charge, by quoting the publication citation and the deposition numbers 817379 (**3**), 817683 (**4**), and 817924 (**5**).

Supporting Online Material

www.sciencemag.org/cgi/content/full/333/6043/733/DC1
Materials and Methods
SOM Text
Figs. S1 to S7
Table S1 to S8
References (*42*, *43*)

24 March 2011; accepted 5 July 2011
10.1126/science.1206036

Spectroscopic Observation of Dual Catalytic Sites During Oxidation of CO on a Au/TiO_2 Catalyst

Isabel Xiaoye Green,[1] Wenjie Tang,[2] Matthew Neurock,[1,2] John T. Yates Jr.[1,2]*

The prevailing view of CO oxidation on gold-titanium oxide (Au/TiO_2) catalysts is that the reaction occurs on metal sites at the Au/TiO_2 interface. We observed dual catalytic sites at the perimeter of 3-nanometer Au particles supported on TiO_2 during CO oxidation. Infrared-kinetic measurements indicate that O-O bond scission is activated by the formation of a $CO\text{-}O_2$ complex at dual Ti-Au sites at the Au/TiO_2 interface. Density functional theory calculations, which provide the activation barriers for the formation and bond scission of the $CO\text{-}O_2$ complex, confirm this model as well as the measured apparent activation energy of 0.16 electron volt. The observation of sequential delivery and reaction of CO first from TiO_2 sites and then from Au sites indicates that catalytic activity occurs at the perimeter of Au nanoparticles.

The catalytic behavior of Au/TiO_2 contrasts with the inactivity of separate bulk Au and oxide surfaces, as was first recognized in the pioneering work of Haruta and co-workers (*1*, *2*) and in the subsequent applications by others (*3*). Multiple mechanisms have been proposed to explain the high catalytic activity of oxide-supported Au for CO oxidation at low temperatures, but there is little consensus on the nature of the active sites or the details of the reaction mechanism (*3*–*6*). Although the catalytic importance of the perimeter has been recognized, the role of the support is still generally overlooked. Reactions, and in particular CO oxidation, are thought to occur on Au sites at the perimeter, whereas the support sites are only thought to be involved in stabilizing O_2 at the interface (*7*–*14*). The direct reaction of O_2 and CO on TiO_2 sites that are adjacent to Au particles has not been considered, because weak binding of CO occurs on supports such as TiO_2 (*15*, *16*). Although it was reported that CO does not adsorb on smooth Au terrace sites (*17*), the CO adsorption on coordinatively unsaturated Au sites is stronger than on TiO_2 (*2*, *18*, *19*), leading to the view that Au delivers CO to active sites for the catalytic process.

The experiments and theoretical results reported here require the reconsideration of this fundamentally important issue where just the opposite behavior has been found. We have carried out CO oxidation over a Au/TiO_2 catalyst at low temperatures, where CO is chemisorbed on both Au and TiO_2 sites and can be separately observed on these sites during reaction. We used in situ infrared spectroscopy to follow the kinetic changes at both Au and TiO_2 sites that reside at the periphery of the Au/TiO_2 interface. On the basis of these experimental findings and the results from density functional theory (DFT) calculations, we propose a low-temperature mechanism for the operation of dual Au/TiO_2 catalytic sites at the perimeter of Au nanoparticles.

We studied gold clusters (~2-nm to ~8-nm diameter, with a most probable diameter of 3 nm) supported on high-surface-area powdered TiO_2 by transmission infrared (IR) spectroscopy (*20*) (fig. S1). Gold clusters of this size are reported to be the most active for CO oxidation, both in actual supported Au catalysts (*2*, *6*, *21*) as well as for model catalysts made by vacuum deposition of Au clusters on single crystal films of TiO_2 (Au/TiO_2) (*22*). The chemical deposition-precipitation methods are described in (*20*), and an electron micrograph of the catalyst after the CO oxidation experiments is shown in fig. S2. The temperature range we have worked at (110

[1]Department of Chemistry, University of Virginia, Charlottesville, VA 22904, USA. [2]Department of Chemical Engineering, University of Virginia, Charlottesville, VA 22904, USA.

*To whom correspondence should be addressed. E-mail: johnt@virginia.edu